Viser Technology Pte. Ltd.
Mechanical Engineering Science
doi: 10.33142/mes.v2i2.3160

Research Article Open Access

Robust Sliding Mode Control for a 2-DOF Lower Limb Exoskeleton Base on Linear Extended State Observer

Zhenlei CHEN[1, 2], Qing GUO[1, 2*], Yao YAN[1, 2], Dan JIANG[3]

1 School of Aeronautics and Astronautics, University of Electronic Science and Technology of China, Chengdu, China
2 Aircraft Swarm Intelligent Sensing and Cooperative Control Key Laboratory of Sichuan Province, Chengdu, China
3 School of Mechanical and Electrical Engineering, University of Electronic Science and Technology of China, Chengdu, China

***Corresponding Author:** Qing GUO, guoqinguestc@163.com*

Abstract:
For the 2- Degree of Freedom (DOF) lower limb exoskeleton, to ensure the system robustness and dynamic performance, a linear-extended-state-observer-based (LESO) robust sliding mode control is proposed to not only reduce the influence of parametric uncertainties, unmodeled dynamics, and external disturbance but also estimate the unmeasurable real-time joint angular velocity directly. Then, via Lyapunov technology, the stability of the corresponding LESO and controller is proven. The appropriate and reasonable simulation was carried out to verify the effectiveness of the proposed LESO and exoskeleton controller.

Keywords: *lower limb exoskeleton; linear-extended-state-observer; robust sliding model control; uncertain nonlinearity*

1 Introduction

For the 2- Degree of Freedom (DOF) lower limb exoskeleton, a linear-With the development of the world economy, and the improvement of human living level, wearable robots have played the key role in the field of medical rehabilitation and industrial production. The exoskeleton, a typical wearable robot, can help specific groups of people complete specific human-machine collaboration tasks, such as assisting hemiplegic patients with rehabilitation training or assisting workers to complete heavy tasks. However, since the complexity and fragility of the human environment, the requirements for the dynamic performance and robustness of the exoskeleton robot are relatively high.

To improve the robustness and dynamic tracking performance of the exoskeleton robot system, many advanced nonlinear controllers have been investigated, such as fuzzy adaptive control [1], repetitive learning control [2], RBFNN adaptive control [3], and discrete-time extended state observer-based intelligent PD control [4]. The training mechanism has been roughly divided into two categories for the exoskeleton: active mechanism and passive mechanism [5]. More specifically, the designed training trajectory is predefined for the passive mechanism without considering the real-time human motion intention [6-7]. Conversely, the training trajectory is designed based on the current human's motion intention for the active mode. The impedance control [8] and admittance control [9] usually are adopted to ensure compliance between humans and the exoskeleton. Li *et al.* [10] assumed admittance control to deal with a human subject's intention. Yu *et al.* [11] proposed an adaptive impedance control strategy to compensate for dynamic uncertainties.

To deal with the parameter uncertainty and external disturbance, designing the related observer to estimate the unknown form is used as the controller design compensation. The disturbance observer mainly includes sliding mode disturbance observer [12], extended state observer (ESO) [13], and so on. In [14], an extended state observer-based integral sliding mode control is adopted in the underwater robot. For the electro-hydraulic system, Guo *et al.* [15] proposed an ESO-based backstepping controller. Furthermore, Sun *et al.* [16] proposed a sliding-mode-disturbance-observer-based tracking control strategy for Euler–Lagrange systems modeling uncertainties and external disturbances.

In this paper, as shown in figure 1, to improve the robustness and dynamic performance of the 2-DOF lower limb exoskeleton, a linear-extended-state-observer-based (LESO) robust sliding mode control is proposed to estimate the unmeasurable joint angular velocity and the error consisting of dynamic deviation and external disturbance. Finally, the related simulation experiment was carried out to verify the effectiveness of the controller.

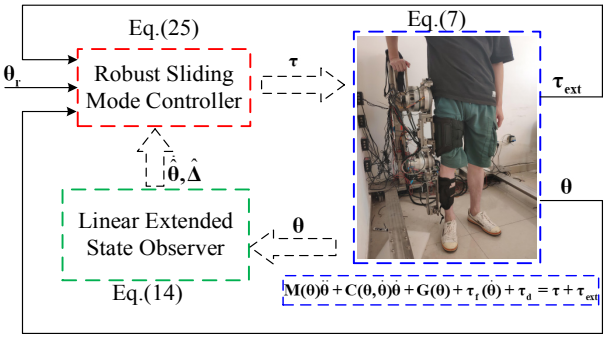

Figure 1 Robust sliding mode control diagram of 2-DOF lower limb exoskeleton

2 Sliding Mode Control for 2-DOF Lower Limb Exoskeleton

2.1 Dynamic of the 2-DOF lower limb exoskeleton

The 2-DOF lower limb exoskeleton that needs to be modeled is shown in the right subgraph of figure 2. According to the human lower limb's physiological structure, the mechanical structure of the prototype is composed of thigh arm, shank arm, hip joint motor, and knee joint motor, and the hip joint motor is fixed on the bracket. Then, the operator and exoskeleton are connected by the bandage and 3-Dimension (3-D) force sensor. Furthermore, the real-time joint position is measured by the absolute encoder, but the joint velocity is measured directly.

At figure 2, O represents the origin of the coordinate system, $\theta_1$and $\theta_2$denote the angular positions of the hip joint and knee joint, $m_{th}$and m_{sh}denote the weights of the thigh arm and shank arm, $a_{th}$and a_{sh}denote the length of the thigh arm and shank arm, $l_{th}$and l_{sh}denote the centroid distance, and g denote the gravity constant.

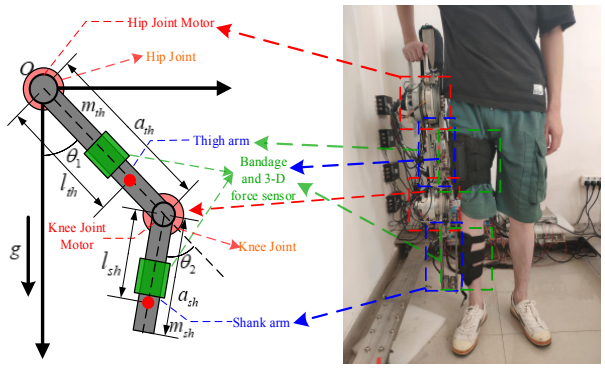

Figure 2 Mechanical structure diagram and physical diagram of 2-DOF lower limb exoskeleton.

According to the [17], the ideal Lagrangian dynamic of the exoskeleton with human-robot interaction and joint friction is model as

$$\mathbf{M}(\boldsymbol{\theta})\ddot{\boldsymbol{\theta}}+\mathbf{C}(\boldsymbol{\theta},\dot{\boldsymbol{\theta}})\dot{\boldsymbol{\theta}}+\mathbf{G}(\boldsymbol{\theta})+\boldsymbol{\tau}_f(\dot{\boldsymbol{\theta}})=\boldsymbol{\tau}+\boldsymbol{\tau}_{ext} \tag{1}$$

where the $\boldsymbol{\theta}=[\theta_1;\theta_2]$ denote the joint angular position, $\boldsymbol{\tau}\in\mathbb{R}^2$denote the joint driving torque, $\boldsymbol{\tau}_{ext}\in\mathbb{R}^2$denote the real-time human-robot interaction torque.$\mathbf{M}(\boldsymbol{\theta})\in\mathbb{R}^{2\times2}$, $\mathbf{C}(\boldsymbol{\theta},\dot{\boldsymbol{\theta}})\in\mathbb{R}^{2\times2}and\mathbf{G}(\boldsymbol{\theta})\in\mathbb{R}^2$ are the symmetric and positive definite inertia matrix, Coriolis matrix and gravity torque in joint space, and the specific forms is shown as follow

$$\mathbf{M}(\boldsymbol{\theta})=\begin{bmatrix} I_{th}+I_{sh}+m_{th}l_{th}^2+m_{sh}a_{th}^2+m_{sh}l_{sh}^2+2m_{sh}a_{th}l_{sh}\cos\theta_2 & I_{sh}+m_{sh}a_{th}l_{sh}\cos\theta_2+m_{sh}l_{sh}^2 \\ I_{sh}+m_{sh}l_{sh}^2+m_{sh}a_{th}l_{sh}\cos\theta_2 & I_{sh}+m_{sh}l_{sh}^2 \end{bmatrix} \tag{2}$$

$$\mathbf{C}(\boldsymbol{\theta},\dot{\boldsymbol{\theta}})=\begin{bmatrix} -2m_{sh}a_{th}l_{sh}\sin\theta_2\dot{\theta}_2 & -m_{sh}a_{th}l_{sh}\sin\theta_2\dot{\theta}_2 \\ m_{sh}a_{th}l_{sh}\sin\theta_2\dot{\theta}_1 & 0 \end{bmatrix} \tag{3}$$

$$\mathbf{G}(\boldsymbol{\theta})=\begin{bmatrix} l_{th}m_{th}g\sin\theta_1+m_{sh}a_{th}g\sin\theta_1+l_{sh}m_{sh}g\sin(\theta_1+\theta_2) \\ l_{sh}m_{sh}g\sin(\theta_1+\theta_2) \end{bmatrix} \tag{4}$$

Furthermore, $\boldsymbol{\tau}_f(\dot{\boldsymbol{\theta}})\in\mathbb{R}^2$ is adopted to describe hip and knee joint friction, which is shown as

$$\boldsymbol{\tau}_f(\dot{\boldsymbol{\theta}})=\begin{bmatrix} k_{1,1}\,\mathrm{sgn}(\dot{\theta}_1)+k_{1,2}\dot{\theta}_1 \\ k_{2,1}\,\mathrm{sgn}(\dot{\theta}_2)+k_{2,2}\dot{\theta}_2 \end{bmatrix} \tag{5}$$

where $k_{1,1}$and $k_{2,1}$ are the coulomb friction coefficient, $k_{1,2}$ and $k_{2,2}$ are the viscous friction coefficient, respectively.

Generally speaking, the minimum inertia parameter from,

$$\mathbf{M}(\boldsymbol{\theta})\ddot{\boldsymbol{\theta}}+\mathbf{C}(\boldsymbol{\theta},\dot{\boldsymbol{\theta}})\dot{\boldsymbol{\theta}}+\mathbf{G}(\boldsymbol{\theta})+\boldsymbol{\tau}_f(\dot{\boldsymbol{\theta}})=\mathbf{Y}(\boldsymbol{\theta},\dot{\boldsymbol{\theta}},\ddot{\boldsymbol{\theta}})\boldsymbol{\Phi} \tag{6}$$

where $\mathbf{Y}\in\mathbb{R}^{2\times8}$ and $\boldsymbol{\Phi}\in\mathbb{R}^8$ denote the regression matrix and unknown parameter vector. Further, according to the dataset, $\boldsymbol{\Phi}$ can be obtained by many algorithms, such as least squares method, ridge regression or heuristic algorithm.

2.2 Linear Extended State Observer Design

In this paper, the nominal values of the parameter vector $\boldsymbol{\Phi}$ are utilized in the linear extended state observer and sliding mode controller designed, which usually is obtained by model parameter identification or generated by CAD software, such as SolidWorks and so on. However, the value of the parameter vector obtained by the above methods is often inaccurate in practice. Meanwhile, external disturbance may also affect the dynamic performance of the exoskeleton system. To address this problem, the LESO is designed to ensure the robustness of the 2-DOF lower limb exoskeleton. Considering the external disturbance , the real dynamic can be described as follow:

$$\mathbf{M}(\boldsymbol{\theta})\ddot{\boldsymbol{\theta}}+\mathbf{C}(\boldsymbol{\theta},\dot{\boldsymbol{\theta}})\dot{\boldsymbol{\theta}}+\mathbf{G}(\boldsymbol{\theta})+\boldsymbol{\tau}_f(\dot{\boldsymbol{\theta}})+\boldsymbol{\tau}_d=\boldsymbol{\tau}+\boldsymbol{\tau}_{ext} \tag{7}$$

Assumption 1: The parameter matrices or vectors $\mathbf{M}(\boldsymbol{\theta})$, $\mathbf{C}(\boldsymbol{\theta},\dot{\boldsymbol{\theta}})$, $\mathbf{G}(\boldsymbol{\theta})$ and $\boldsymbol{\tau}_f(\dot{\boldsymbol{\theta}})$can be expressed as follow:

$$\begin{cases} \mathbf{M}(\boldsymbol{\theta})=\mathbf{M}_0(\boldsymbol{\theta})+\mathbf{M}_\Delta(\boldsymbol{\theta}), & \mathbf{C}(\boldsymbol{\theta},\dot{\boldsymbol{\theta}})=\mathbf{C}_0(\boldsymbol{\theta},\dot{\boldsymbol{\theta}})+\mathbf{C}_\Delta(\boldsymbol{\theta},\dot{\boldsymbol{\theta}}), \\ \mathbf{G}(\boldsymbol{\theta})=\mathbf{G}_0(\boldsymbol{\theta})+\mathbf{G}_\Delta(\boldsymbol{\theta}), & \boldsymbol{\tau}_f(\dot{\boldsymbol{\theta}})=\boldsymbol{\tau}_{f,0}(\dot{\boldsymbol{\theta}})+\boldsymbol{\tau}_{f,\Delta}(\dot{\boldsymbol{\theta}}). \end{cases} \tag{8}$$

where $\mathbf{M}_0(\boldsymbol{\theta})$, $\mathbf{C}_0(\boldsymbol{\theta},\dot{\boldsymbol{\theta}})$, $\mathbf{G}_0(\boldsymbol{\theta})$ and $\boldsymbol{\tau}_{f,0}(\dot{\boldsymbol{\theta}})$ are the nominal and known matrices and vectors, and $\mathbf{M}_0(\boldsymbol{\theta})$ is the symmetric and positive definite matrices. Meanwhile, the $\mathbf{M}_\Delta(\boldsymbol{\theta})$, $\mathbf{C}_\Delta(\boldsymbol{\theta},\dot{\boldsymbol{\theta}})$, $\mathbf{G}_\Delta(\boldsymbol{\theta})$ and $\boldsymbol{\tau}_{f,\Delta}(\dot{\boldsymbol{\theta}})$ are the unknown matrices.

Hence, (8) can be rewritten as

$$\mathbf{M}_0(\boldsymbol{\theta})\ddot{\boldsymbol{\theta}}+\mathbf{C}_0(\boldsymbol{\theta},\dot{\boldsymbol{\theta}})\dot{\boldsymbol{\theta}}+\mathbf{G}_0(\boldsymbol{\theta})+\boldsymbol{\tau}_{f,0}(\dot{\boldsymbol{\theta}})+\Delta=\boldsymbol{\tau}+\boldsymbol{\tau}_{ext} \tag{9}$$

where the error Δ denotes the lumped uncertainty, which is defined as

$$\Delta=\mathbf{M}_\Delta(\boldsymbol{\theta})\ddot{\boldsymbol{\theta}}+\mathbf{C}_\Delta(\boldsymbol{\theta},\dot{\boldsymbol{\theta}})\dot{\boldsymbol{\theta}}+\mathbf{G}_\Delta(\boldsymbol{\theta})+\boldsymbol{\tau}_{f,\Delta}(\dot{\boldsymbol{\theta}})+\boldsymbol{\tau}_d \tag{10}$$

For the 2-DOF lower limb exoskeleton system, defined state variables as $\mathbf{x}=[\mathbf{x}_1,\mathbf{x}_2]^T=[\boldsymbol{\theta},\dot{\boldsymbol{\theta}}]$. Consequently, the corresponding state space model is expressed as follow

$$\begin{cases} \dot{\mathbf{x}}_1=\mathbf{x}_2 \\ \dot{\mathbf{x}}_2=\mathbf{M}_0^{-1}\left(\boldsymbol{\tau}+\boldsymbol{\tau}_{ext}-\mathbf{C}_0\mathbf{x}_2-\mathbf{G}_0-\boldsymbol{\tau}_{f,0}\right)-\mathbf{M}_0^{-1}\Delta \end{cases} \tag{11}$$

In order to accomplish the design missions discussed in Section 2.1, the addition lumped uncertainty $\mathbf{M}_0^{-1}\boldsymbol{\Delta}$ is extended as an additional state variable. Then, the extended state space model can be written as

$$\begin{cases} \dot{\mathbf{x}}_1 = \mathbf{x}_2 \\ \dot{\mathbf{x}}_2 = \mathbf{M}_0^{-1}\left(\boldsymbol{\tau} + \boldsymbol{\tau}_{ext} - \boldsymbol{\varphi}(\mathbf{x}) - \mathbf{G}_0\right) - \mathbf{x}_3 \\ \dot{\mathbf{x}}_3 = \boldsymbol{\delta}(t) \end{cases} \tag{12}$$

where $\boldsymbol{\delta}(t)$ represent the time derivative of the state variable $\mathbf{x}_3, \boldsymbol{\varphi}(\mathbf{x}) = \mathbf{C}_0\mathbf{x}_2 + \boldsymbol{\tau}_f$.

Assumption 2: The function $\boldsymbol{\varphi}(\mathbf{x})$ is global Lipschitz with respecting to $\mathbf{x}_2$ in its practical range; and addition lumped uncertainty $\boldsymbol{\Delta}$and its time derivative $\dot{\boldsymbol{\Delta}}$ are both bounded.

The mission target of the LESO is not only observing the unmeasured state variable $\mathbf{x}_2$but also the estimating the lumped uncertainty state variable $\mathbf{x}_3$ for controller compensation in real time and to guarantee the robustness and dynamic performance of the system.

In this paper, $\hat{\mathbf{x}}_i$(i=1,2,3) denotes the estimate value of state $\mathbf{x}$, and $\tilde{\mathbf{x}}_i = \mathbf{x}_i - \hat{\mathbf{x}}_i$ denotes the estimate error for the i-th state. We rewrite the extended state space model (12) as

$$\dot{\mathbf{x}} = \mathbf{A}_0\mathbf{x} + \mathbf{B}_0\mathbf{u} - \boldsymbol{\Phi}(\mathbf{x}) + \mathbf{D}(t) \tag{13}$$

where

$$\mathbf{A}_0 = \begin{bmatrix} \mathbf{0}_{2\times2} & \mathbf{I}_{2\times2} & \mathbf{0}_{2\times2} \\ \mathbf{0}_{2\times2} & \mathbf{0}_{2\times2} & \mathbf{I}_{2\times2} \\ \mathbf{0}_{2\times2} & \mathbf{0}_{2\times2} & \mathbf{0}_{2\times2} \end{bmatrix}, \quad \mathbf{B}_0 = \begin{bmatrix} \mathbf{0}_{2\times2} \\ \mathbf{M}_0^{-1}(\mathbf{x}) \\ \mathbf{0}_{2\times2} \end{bmatrix}, \quad \boldsymbol{\Phi}(\mathbf{x}) = \begin{bmatrix} \mathbf{0}_{2\times1} \\ \boldsymbol{\varphi}(\mathbf{x}) \\ \mathbf{0}_{2\times1} \end{bmatrix}, \quad \mathbf{D}(t) = \begin{bmatrix} \mathbf{0}_{2\times1} \\ \mathbf{0}_{2\times1} \\ \boldsymbol{\delta}(t) \end{bmatrix},$$

$\mathbf{I}_{2\times2}$ presents a unit matrix with the size of $\boldsymbol{\nu}_{2\times2}$, and $\mathbf{0}_{2\times2}$ presents a zero unit matrix with the size of 2×2.

Then, corresponding LESO model is designed as follows

$$\dot{\hat{\mathbf{x}}} = \mathbf{A}_0\hat{\mathbf{x}} + \mathbf{B}_0\mathbf{u} - \hat{\boldsymbol{\Phi}}(\mathbf{x}) + \mathbf{H}(\mathbf{x}_1 - \hat{\mathbf{x}}_1) \tag{14}$$

where $\hat{\boldsymbol{\Phi}}(\mathbf{x}) = \boldsymbol{\Phi}(\mathbf{x}_1, \mathbf{x}_2) - \boldsymbol{\Phi}(\mathbf{x}_1, \hat{\mathbf{x}}_2)$ denotes the estimate error, $\mathbf{H} = [3\omega_0 \ 3\omega_0^2 \ \omega_0^3]^T$, which $\mathbf{H}$ is the observer gain, $\tilde{\mathbf{X}}$ denotes the a type of observer tuning gain, which is selected as a positive parameter.

Subtract (14) from (13), the state space model of $\tilde{\mathbf{x}}$ is shown as follow

$$\dot{\tilde{\mathbf{x}}} = \mathbf{A}_0\tilde{\mathbf{x}} - \tilde{\boldsymbol{\Phi}}(\mathbf{x}) + \mathbf{D}(t) - \mathbf{H}(\mathbf{x}_1 - \hat{\mathbf{x}}_1) \tag{15}$$

Let $\boldsymbol{\varepsilon}_1 = \tilde{\mathbf{x}}_1$, $\boldsymbol{\varepsilon}_2 = \tilde{\mathbf{x}}_2 / \omega_0$, and $\boldsymbol{\varepsilon}_2 = \tilde{\mathbf{x}}_3 / \omega_0^2$ denote the scaled estimation error, then (15) can be rewritten as

$$\dot{\boldsymbol{\varepsilon}} = \omega_0\mathbf{A}\boldsymbol{\varepsilon} - \mathbf{B}_2\frac{\mathbf{M}_0^{-1}\tilde{\boldsymbol{\varphi}}(\mathbf{x})}{\omega_0} + \mathbf{B}_3\frac{\boldsymbol{\delta}(t)}{\omega_0^2}, \tag{16}$$

where the $\mathbf{A} = \begin{bmatrix} -3*\mathbf{I}_{2\times2} & \mathbf{I}_{2\times2} & \mathbf{0}_{2\times2} \\ -3*\mathbf{I}_{2\times2} & \mathbf{0}_{2\times2} & \mathbf{I}_{2\times2} \\ -\mathbf{I}_{2\times2} & \mathbf{0}_{2\times2} & \mathbf{0}_{2\times2} \end{bmatrix}$, $\mathbf{B}_3 = \begin{bmatrix} \mathbf{0}_{2\times2} \\ \mathbf{0}_{2\times2} \\ \mathbf{I}_{2\times2} \end{bmatrix}$, $\mathbf{B}_3 = \begin{bmatrix} \mathbf{0}_{2\times2} \\ \mathbf{0}_{2\times2} \\ \mathbf{I}_{2\times2} \end{bmatrix}$, and $\boldsymbol{\varepsilon} = [\boldsymbol{\varepsilon}_1 \ \boldsymbol{\varepsilon}_2 \ \boldsymbol{\varepsilon}_3]^T$.

Obviously, matrix $\mathbf{A}$ is Hurwitz. Hence, there exists a positive definite matrix $\mathbf{P}$ satisfying below qualification.

$$\mathbf{A}^T\mathbf{P} + \mathbf{P}\mathbf{A} = -2*\mathbf{I} \tag{17}$$

Theorem 1: For the LESO (14), when the **Assumption 2** hold, the state estimation errors will reach and stay in a predefined region with the appropriate constant ω_0.

Proof of Theorem 1: For the LESO (14), considering the following positive definite Lyapunov function:

$$\mathbf{V}_O = \boldsymbol{\varepsilon}^T\mathbf{P}\boldsymbol{\varepsilon} \tag{18}$$

Then, the time derivative of $\mathbf{V}_O$is

$$\begin{aligned} \dot{\mathbf{V}}_O &= \dot{\boldsymbol{\varepsilon}}^T\mathbf{P}\boldsymbol{\varepsilon} + \boldsymbol{\varepsilon}^T\mathbf{P}\dot{\boldsymbol{\varepsilon}} \\ &= \left(\omega_0\mathbf{A}\boldsymbol{\varepsilon} - \mathbf{B}_2\frac{\mathbf{M}_0^{-1}\tilde{\boldsymbol{\varphi}}(\mathbf{x})}{\omega_0} + \mathbf{B}_3\frac{\boldsymbol{\delta}(t)}{\omega_0^2}\right)^T\mathbf{P}\boldsymbol{\varepsilon} + \boldsymbol{\varepsilon}^T\mathbf{P}\left(\omega_0\mathbf{A}\boldsymbol{\varepsilon} - \mathbf{B}_2\frac{\mathbf{M}_0^{-1}\tilde{\boldsymbol{\varphi}}(\mathbf{x})}{\omega_0} + \mathbf{B}_3\frac{\boldsymbol{\delta}(t)}{\omega_0^2}\right) \\ &= \omega_0\left(\boldsymbol{\varepsilon}^T\mathbf{A}^T\mathbf{P}\boldsymbol{\varepsilon} + \boldsymbol{\varepsilon}^T\mathbf{P}\mathbf{A}\boldsymbol{\varepsilon}\right) + \left(-\mathbf{B}_2\frac{\mathbf{M}_0^{-1}\tilde{\boldsymbol{\varphi}}(\mathbf{x})}{\omega_0} + \mathbf{B}_3\frac{\boldsymbol{\delta}(t)}{\omega_0^2}\right)^T\mathbf{P}\boldsymbol{\varepsilon} + \boldsymbol{\varepsilon}^T\mathbf{P}\left(-\mathbf{B}_2\frac{\mathbf{M}_0^{-1}\tilde{\boldsymbol{\varphi}}(\mathbf{x})}{\omega_0} + \mathbf{B}_3\frac{\boldsymbol{\delta}(t)}{\omega_0^2}\right) \end{aligned} \tag{19}$$

Based on **Assumption 2**, the condition $|\tilde{\boldsymbol{\varphi}}(\mathbf{x})| \le \kappa\|\boldsymbol{\varepsilon}\|$ hold, and (19) can be rewritten as

$$\dot{\mathbf{V}}_O \le \left(-2\omega_0 + 2\frac{\lambda_1\kappa}{\omega_0}\left\|\mathbf{M}_0^{-1}\right\|\right)\|\boldsymbol{\varepsilon}\|^2 + 2\frac{\lambda_2}{\omega_0^2}|\boldsymbol{\delta}(t)|\|\boldsymbol{\varepsilon}\| \tag{20}$$

where $\lambda_i = \|\mathbf{PB}_i\|, \mathbf{i} = \mathbf{2,3}$.

The time derivative of the Lyapunov function (19) is a negative function when (20) is established.

$$\|\boldsymbol{\varepsilon}\| \ge \frac{\lambda_2|\boldsymbol{\delta}(t)|}{\omega_0\left(\omega_0^2 - \lambda_1\kappa\left\|\mathbf{M}_0^{-1}\right\|\right)} \tag{21}$$

Considering (21), when the bandwidth ω_0 is big enough, the estimation error $\|\boldsymbol{\varepsilon}\|$ can quickly converge to a smaller range, which is acceptable in practical applications.

2.3 Robust Sliding Mode Controller Design

In this section, the robust sliding mode controller is adopted based on LESO (14) to ensure the robustness and dynamic performance of the 2-DOF lower limb exoskeleton. For the system state space model (11) and (12), let $\mathbf{x}_r$ express the desired trajectory. Obviously, the objective is to make the tracking error $\mathbf{e}=\mathbf{x}-\mathbf{x}_r$ converge to zero.

Define an auxiliary sliding mode error $\mathbf{s} \in \mathbb{R}^2$ as

$$\mathbf{s} = \dot{\mathbf{e}} + \boldsymbol{\alpha}\mathbf{e} \tag{22}$$

with $\boldsymbol{\alpha} \in \mathbb{R}^{2\times2}$ being a diagonal matrix with positive diagonal element. Then, substituting (11), the time derivative of $\mathbf{s}$ can be shown as

$$\begin{aligned} \dot{\mathbf{s}} &= \ddot{\mathbf{e}} + \boldsymbol{\alpha}\dot{\mathbf{e}} \\ &= \mathbf{M}_0^{-1}\left(\boldsymbol{\tau} + \boldsymbol{\tau}_{ext} - \mathbf{C}_0\mathbf{x}_2 - \mathbf{G}_0 - \boldsymbol{\tau}_{f,0}\right) - \mathbf{M}_0^{-1}\boldsymbol{\Delta} - \ddot{\mathbf{x}}_r + \boldsymbol{\alpha}\left(\mathbf{x}_1 - \ddot{\mathbf{x}}_r\right) \end{aligned} \tag{23}$$

Design a sliding mode tracking controller $\boldsymbol{\tau}$ as

$$\boldsymbol{\tau} = -\mathbf{M}_0\mathbf{K}\mathbf{s} - \boldsymbol{\tau}_{ext} + \mathbf{G}_0 + \boldsymbol{\varphi}(\mathbf{x}) + \boldsymbol{\Delta} + \mathbf{M}_0\ddot{\mathbf{x}}_r - \mathbf{M}\boldsymbol{\alpha}\left(\mathbf{x}_1 - \ddot{\mathbf{x}}_r\right) \tag{24}$$

where $\mathbf{K}$ is the designed positive control gain. $\boldsymbol{\varphi}(\mathbf{x})$ is defined in Section 2.2.

Since value of lumped uncertainty $\boldsymbol{\Delta}$ is unknown and real-time joint angular velocity $\mathbf{x}_2$ is unmeasurable, based on the LESO (14), the robust sliding mode controller is redesigned as

$$\boldsymbol{\tau} = -\mathbf{M}_0\mathbf{K}\hat{\mathbf{s}} - \boldsymbol{\tau}_{ext} + \mathbf{G}_0 + \hat{\boldsymbol{\varphi}}(\mathbf{x}) + \mathbf{M}_0\hat{\mathbf{x}}_3 + \mathbf{M}_0\ddot{\mathbf{x}}_r - \mathbf{M}\boldsymbol{\alpha}\left(\mathbf{x}_1 - \ddot{\mathbf{x}}_r\right) \tag{25}$$

The total Lyapunov function is defined as

$$\mathbf{V} = \frac{1}{2}\mathbf{s}^T\mathbf{s} + \mathbf{V}_O \tag{26}$$

Substituting (23), and it's time derivative is shown as

$$\begin{aligned} \dot{\mathbf{V}} &= \mathbf{s}^T\dot{\mathbf{s}} + \dot{\mathbf{V}}_O \\ &= \mathbf{s}^T\left[\mathbf{M}_0^{-1}\left(\boldsymbol{\tau} + \boldsymbol{\tau}_{ext} - \boldsymbol{\varphi}(\mathbf{x}) - \mathbf{G}_0\right) - \mathbf{M}_0^{-1}\boldsymbol{\Delta} - \ddot{\mathbf{x}}_r + \boldsymbol{\alpha}\left(\mathbf{x}_1 - \ddot{\mathbf{x}}_r\right)\right] + \dot{\mathbf{V}}_O \end{aligned} \tag{27}$$

Substituting (25) into (27), considering Young's inequality, (27) can be rewritten as

$$\begin{aligned} \dot{\mathbf{V}} &= -\mathbf{s}^T\mathbf{K}\mathbf{s} + \mathbf{s}^T\mathbf{K}\tilde{\mathbf{s}} + \mathbf{s}^T\left[-\mathbf{M}_0^{-1}\tilde{\boldsymbol{\varphi}}(\mathbf{x}) + \tilde{\mathbf{x}}_3 + \boldsymbol{\alpha}\tilde{\mathbf{x}}_2\right] + \dot{\mathbf{V}}_O \\ &= -\mathbf{s}^T\mathbf{K}\mathbf{s} + \mathbf{s}^T\left[(\mathbf{K}+\boldsymbol{\alpha})\tilde{\mathbf{x}}_2 - \mathbf{M}_0^{-1}\tilde{\boldsymbol{\varphi}}(\mathbf{x}) + \tilde{\mathbf{x}}_3\right] + \dot{\mathbf{V}}_O \\ &\le -\mathbf{s}^T\mathbf{K}\mathbf{s} + \mathbf{s}^T\left[(\mathbf{K}+\boldsymbol{\alpha})\tilde{\mathbf{x}}_2 - \mathbf{M}_0^{-1}\tilde{\boldsymbol{\varphi}}(\mathbf{x}) + \tilde{\mathbf{x}}_3\right] + \left(-2\omega_0 + 2\frac{\lambda_1\kappa}{\omega_0}\left\|\mathbf{M}_0^{-1}\right\|\right)\|\boldsymbol{\varepsilon}\|^2 + 2\frac{\lambda_2}{\omega_0^2}|\boldsymbol{\delta}(t)|\|\boldsymbol{\varepsilon}\| \\ &\le -\mathbf{s}^T\left(\mathbf{K} - \frac{1}{2}\mathbf{I}\right)\mathbf{s} + \frac{1}{2}\tilde{\boldsymbol{\Delta}}_{dis}^T\tilde{\boldsymbol{\Delta}}_{dis} + \left(-2\omega_0 + 2\frac{\lambda_1\kappa}{\omega_0}\left\|\mathbf{M}_0^{-1}\right\|\right)\|\boldsymbol{\varepsilon}\|^2 + 2\frac{\lambda_2}{\omega_0^2}|\boldsymbol{\delta}(t)|\|\boldsymbol{\varepsilon}\| \end{aligned} \tag{28}$$

where $\tilde{\boldsymbol{\Delta}}_{dis} = (\mathbf{K}+\boldsymbol{\alpha})\tilde{\mathbf{x}}_2 - \mathbf{M}_0^{-1}\tilde{\boldsymbol{\varphi}}(\mathbf{x}) + \tilde{\mathbf{x}}_3$, which expresses the

lumped estimated error term.

Considering the discussion of LESO (14) in section 2.2 and (28), the amplitude of $\tilde{\boldsymbol{\Delta}}_{dis}^{T}\tilde{\boldsymbol{\Delta}}_{dis}$ is determined by the performance of LESO (14), which is related to the value of parameter $\boldsymbol{\omega}_0$. Meanwhile, the rate of convergence depends on control gain $\mathbf{K}$ and observer bandwidth $\boldsymbol{\omega}_0$. Then, if $\mathbf{K}$ is large enough and $\boldsymbol{\omega}_0$ is big enough, the satisfactory tracking effect can be obtained.

3 Simulation

In order to verify the effectiveness of the proposed robust sliding mode control, the simulation model is built to realize the passive mechanism of exoskeleton by Matlab/Simulink, which is shown in figure 3.

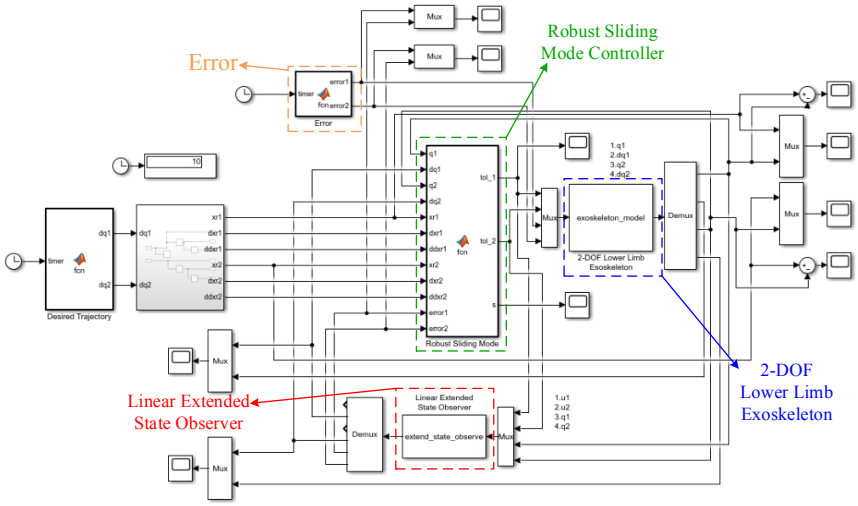

Figure 3 Configuration of the simulation for the 2-DOF lower limb exoskeleton

Then, the dynamic model of 2-DOF lower limb exoskeleton is set as follows

$$\mathbf{M}_0(\boldsymbol{\theta})\ddot{\boldsymbol{\theta}}+\mathbf{C}_0(\boldsymbol{\theta},\dot{\boldsymbol{\theta}})\dot{\boldsymbol{\theta}}+\mathbf{G}_0(\boldsymbol{\theta})+\boldsymbol{\tau}_{f,0}(\dot{\boldsymbol{\theta}})+\Delta=\boldsymbol{\tau}+\boldsymbol{\tau}_{ext} \tag{29}$$

where, $\mathbf{M}_0=[27.22+3.32\cos\theta_2, 8.28+1.66\cos\theta_2; 8.28+1.66\cos\theta_2, 8.28]$ $\mathbf{C}_0=[-3.32\sin\theta_2\dot{\theta}_2, -1.66\sin\theta_2\dot{\theta}_2; 1.66\sin\theta_2\dot{\theta}_1, 0]$ $\mathbf{G}_0=[41.76\sin(\theta_1+\theta_2)+184.92\sin\theta_1; 41.76\sin(\theta_1+\theta_2)]$, $\boldsymbol{\tau}_{f,0}=[27.81\,\mathrm{sgn}(\theta_1)+24.09\theta_1;\ 37.24\,\mathrm{sgn}(\theta_2)+41.38\theta_2]$ Δ is designed as follow

$$\begin{cases}\Delta_1 = \frac{1}{2}\sin(\frac{3}{2}\pi t);\\ \Delta_2 = \frac{1}{2}\sin(\frac{3}{2}\pi t+\frac{1}{2}\pi);\end{cases} \tag{30}$$

Then, according to the controller (25), the human-robot interaction torque $\boldsymbol{\tau}_{ext}$ is challenging to design and will be compensated by the controller so $\boldsymbol{\tau}_{ext}$ is set as 0 in the simulation experiment. Furthermore, the desirable trajectory $\boldsymbol{\theta}_r$ of the exoskeleton is set as the human natural walking gait given by

$$\begin{cases}\theta_{r,1}=\sum_{k=1}^{4}\left(a_{k,1}\sin(k\omega t)+b_{k,1}\cos(k\omega t)\right)+\theta_{0,1};\\ \theta_{r,2}=\sum_{k=1}^{4}\left(a_{k,2}\sin(k\omega t)+b_{k,2}\cos(k\omega t)\right)+\theta_{0,2};\end{cases} \tag{31}$$

where $\omega=0.4\pi$, $b_{k,1}(k=1,2,3,4)$ are -2.874, -2.423, 1.227 and -0.1462, $b_{k,1}(k=1,2,3,4)$ are 18.52, -2.016, -0.3704 and 0.201, $\theta_{0,1}=10.07$, $b_{k,2}(k=1,2,3,4)$ are 17.62, -2.469, -3.82 and -0.1346, $b_{k,2}(k=1,2,3,4)$ are -1.494, 11.72, 1.014 and 0.2165, and $\theta_{0,2}=-17.49$.

With considering the gait trajectory (31), the parameters of robust sliding mode controller are set as $\boldsymbol{\alpha}=\mathrm{diag}\{25,25\}$, $\mathbf{K}=\mathrm{diag}\{1000,1000\}$. Meanwhile, the parameter of LESO is set as $\boldsymbol{\omega}_0=\mathrm{diag}\{1000,1000\}$. Then, in simulation experiment, the simulation step is set as 0.001 sec.

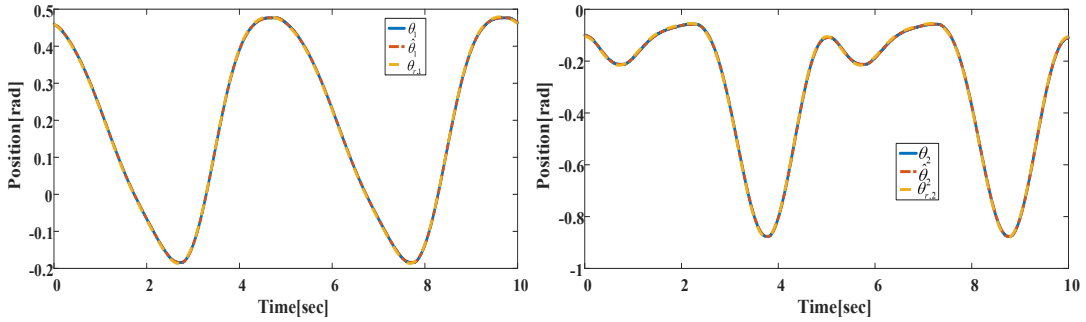

Figure 4 Tracking performance and estimating performance of two joint position trajectories

Figure 4 shows the desired trajectory $\theta_r=[\theta_{r,1},\theta_{r,2}]^T$, estimating trajectory $\hat{\theta}=[\theta_1,\theta_2]^T$, and actual trajectory $|e_1|<3.2\times10^{-3}$ of two joints. Then, the tracking deviation $|e_1|<3.2\times10^{-3}$ and $|e_2|<5.8\times10^{-3}$, and the estimating deviation $|\theta_1-\hat{\theta}_1|<2.4\times10^{-9}$ and $|\theta_2-\hat{\theta}_2|<2.4\times10^{-9}$. It can be seen that the tracking performance of controller and the

estimating performance of the LESO are satisfactory.

Figure 5 shows the setting lumped uncertainty $\boldsymbol{\Delta}=[\Delta_1,\Delta_2]^T$ and estimating lumped uncertainty $\hat{\boldsymbol{\Delta}}=[\hat{\Delta}_1,\hat{\Delta}_2]^T$ of two joints. More specifically, the estimating deviation of lumped uncertainty $|\Delta_1|\le 7.1\times10^{-3}$ and $|\Delta_2|\le 7.2\times10^{-3}$ It can be seen that the lumped uncertainty estimating performance of the LESO are satisfactory.

Figure 6 shows the actual velocity trajectory $\dot{\theta}=[\dot{\theta}_1,\dot{\theta}_2]^T$ and estimating velocity trajectory $\dot{\hat{\theta}}=[\dot{\hat{\theta}}_1,\dot{\hat{\theta}}_2]^T$ of two joints. More specifically, the estimating deviation of $\left|\dot{\theta}_1-\dot{\hat{\theta}}_1\right|<7.07\times10^{-6}$ and $\left|\dot{\theta}_2-\dot{\hat{\theta}}_2\right|<7.07\times10^{-6}$ It can be seen that the velocity deviation estimating performance of the LESO are satisfactory.

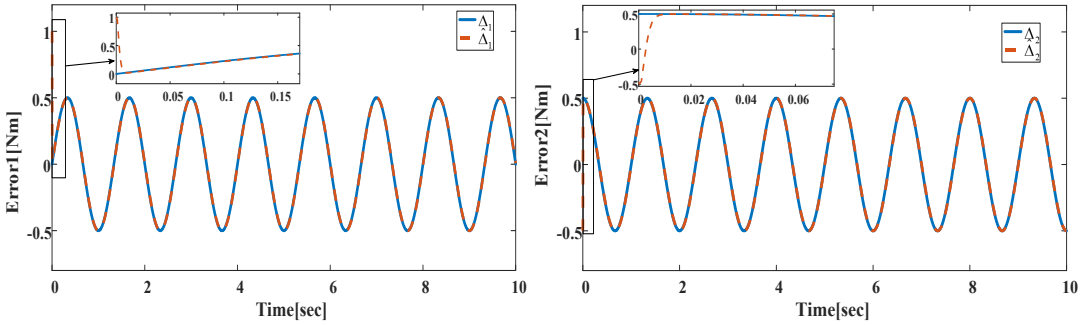

Figure 5 Estimating performance of the lumped uncertainty of two joints

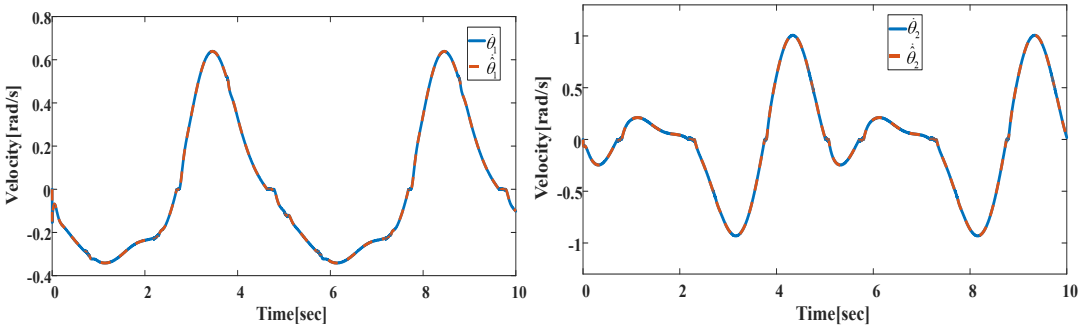

Figure 6 Estimating performance of two joint velocity trajectories

4 Conclusion

In this paper, a LESO-based robust sliding mode controller (25) is designed to improve the robustness and dynamic performance, and the LESO (14) is designed to estimate the unmeasurable state variable and lumped uncertainty consisting of parametric uncertainties, unmodeled dynamics, and external disturbance. For the exoskeleton controller designed, system state estimation and disturbance compensation are adopted to ensure the system's robustness and dynamic performance. For further research plans, the nonlinear ESO will be considered in the exoskeleton controller designed.

Author Contributions: Zhenlei CHEN: Writing draft, Implement, Data verification; Qing GUO: Conceptualization, Methodology; Yao YAN: Result Checking; Dan JIANG: Validation.

Conflict of Interest: The authors declare that they have no competing interests.

Acknowledgments: This work was supported by National Natural Science Foundation of China (No. 51775089 and 11872147), Sichuan Science and Technology Program (No. 2018JY0565 and 2020YFG0137).

References

[1] Li Z, Su C Y, Li G, et al. Fuzzy approximation-based adaptive backstepping control of an exoskeleton for human upper limbs[J]. IEEE Transactions on Fuzzy Systems, 2014, 23(3), 555-566.

[2] Yang Y, Ma L, Huang D. Development and repetitive learning control of lower limb exoskeleton driven by electrohydraulic actuators[J]. IEEE transactions on industrial electronics, 2016, 64(5), 4169-4178.

[3] He W, Li Z, Dong Y, et al. Design and adaptive control for an upper limb robotic exoskeleton in presence of input saturation[J]. IEEE transactions on neural networks and learning systems, 2018, 30(1), 97-108.

[4] Han S, Wang H, Tian Y. A linear discrete-time extended state observer-based intelligent PD controller for a 12 DOFs lower limb exoskeleton LLE-RePA[J]. Mechanical Systems and Signal Processing, 2020, 138, 106547.

[5] Meng W, Liu Q, Zhou Z, et al. Recent development of mechanisms and control strategies for robot-assisted lower limb rehabilitation[J]. Mechatronics, 2015, 31, 132-145.

[6] Hussain S, Xie S Q, Jamwal P K. Robust nonlinear control of an intrinsically compliant robotic gait training orthosis[J]. IEEE Transactions on Systems, Man, and Cybernetics: Systems, 2012, 43(3), 655-665.
[7] Saglia J A, Tsagarakis N G, Dai J S, et al. Control strategies for patient-assisted training using the ankle rehabilitation robot (ARBOT)[J]. IEEE/ASME Transactions on Mechatronics, 2012, 18(6), 1799-1808.
[8] Hogan N. Impedance control: An approach to manipulation. 1984 American control conference. IEEE, 1984, 304-313.
[9] Keemink A Q L, van der Kooij H, Stienen A H A. Admittance control for physical human–robot interaction. The International Journal of Robotics Research, 2018, 37(11), 1421-1444.
[10] Li Z, Huang B, Ye Z, et al. Physical human–robot interaction of a robotic exoskeleton by admittance control[J]. IEEE Transactions on Industrial Electronics, 2018, 65(12), 9614-9624.
[11] Yu X, He W, Li Y, et al. Bayesian Estimation of Human Impedance and Motion Intention for Human-Robot Collaboration. IEEE Transactions on Cybernetics, 2019.
[12] Na J, Ren X, Zheng D. Adaptive control for nonlinear pure-feedback systems with high-order sliding mode observer[J]. IEEE transactions on neural networks and learning systems, 2013, 24(3), 370-382.
[13] Guo B Z, Zhao Z. On the convergence of an extended state observer for nonlinear systems with uncertainty[J]. Systems & Control Letters, 2011, 60(6), 420-430.
[14] Cui R, Chen L, Yang C, et al. Extended state observer-based integral sliding mode control for an underwater robot with unknown disturbances and uncertain nonlinearities[J]. IEEE Transactions on Industrial Electronics, 2017, 64(8), 6785-6795.
[15] Guo Q, Zhang Y, Celler B G, et al. Backstepping control of electro-hydraulic system based on extended-state-observer with plant dynamics largely unknown[J]. IEEE Transactions on industrial Electronics, 2016, 63(11), 6909-6920.
[16] Sun T, Cheng L, Wang W, et al. Semiglobal exponential control of Euler–Lagrange systems using a sliding-mode disturbance observer[J]. Automatica, 2020, 112, 108677.
[17] Siciliano B, Sciavicco L, Villani L, et al. Robotics: modelling, planning and control. Springer Science & Business Media, 2010: 2.